



Unrevealing mechanism of the thermal tautomerization of avobenzone by means of quantum chemical computations

MARKO KOJIĆ, MILENA PETKOVIĆ[#] and MIHAJLO ETINSKI*[#]

Faculty of Physical Chemistry, University of Belgrade, Studentski trg 12–16,
P. O. Box 47, 11158 Belgrade, Serbia

(Received 31 May, revised 17 July, accepted 21 September 2016)

Abstract: Avobenzone (1-(4-*tert*-butylphenyl)-3-(4-methoxyphenyl)propane-1,3-dione) is one of the most widely used UV-A filters in cosmetic sunscreens. The reactivity of avobenzone is complex and challenging to understand, due to a presence of transient tautomers. In this contribution, the chelated enol, rotamer and keto tautomers of a reduced model of avobenzone, which are involved in keto–enol tautomerization, were studied. Two thermal tautomerization mechanisms are postulated and their transient structures are discussed. The computed vertical and adiabatic electronic excitation energies of the tautomers provide an additional insight into the excited state properties of the tautomers.

Keywords: excited states; density functional theory; photochemistry.

INTRODUCTION

Ultraviolet (UV) light is harmful for skin cells since it can damage genetic material.^{1–3} The ozone layer absorbs radiation below 290 nm and thus cosmetic sunscreens need to filter radiation in UV-A (320–380 nm) and UV-B (290–320 nm) bands. Although there are many available UV-B filters, proper UV-A filters are deficient. 1-(4-*tert*-Butylphenyl)-3-(4-methoxyphenyl)propane-1,3-dione (trade name avobenzone (AB)) is the most widely used UV-A absorber in cosmetic sunscreens.⁴ Despite its importance as a UV-A absorber, the photodynamics of AB are not completely understood.^{5–20} This is due to a fact that photo-excited AB transforms into several transient tautomeric forms the lifetimes of which range from ps to ms.^{10,15,18–20} These tautomerizations together with photo-degradation are responsible for a complete loss of UV-A protection under irradiation.

* Corresponding author. E-mail: etinski@ffh.bg.ac.rs

[#] Serbian Chemical Society member.

doi: 10.2298/JSC160531085K

AB is a β -dicarbonyl compound that undergoes keto–enol tautomerization. Generally, the chelated enol form of dibenzoylmethane derivatives are more stable due to an intramolecular hydrogen bond,²¹ although the keto tautomer is also present to a minor extent at equilibrium.²² A quasi-aromatic system of the chelated enol is responsible for the strong absorption band in the UV-A region. On the other hand, the keto tautomer absorbs in the UV-C band,¹⁵ which is not useful for photoprotection.¹⁵ Photochemical investigations showed that a triplet state of the keto tautomer is responsible for photodegradation of AB,^{10,14} which proceeds mainly *via* α -bond cleavages of the carbonyl groups.⁸ Yamaji and Kida performed steady-state and laser flash photolysis experiments in order to examine the photothermal tautomerization of AB in various solvents.¹⁵ The authors observed that upon photoexcitation of the chelated enol, the keto tautomer was produced only in acetonitrile solution but not in other solvents, such as methanol, ethanol, benzene, cyclohexane and dimethyl sulfoxide. The quantum yield of phototautomerization was estimated to be 0.014. The reverse phototautomerization to the chelated enol form was not observed. Several other studies revealed that AB and its derivatives, besides two tautomeric forms, could exist as short-lived enol tautomers (rotamers).^{5,7,9–11,18–20} These tautomers are formed during photoexcitation of the chelated enol tautomer. Cantrell and McGarvey¹⁰ as well as Andrae *et al.*⁹ proposed that these transient species were either produced by rotation about the single C₁–C₂ bond or rotation about the double C₁=C₃ bond.

The aim of the present study was to examine the mechanism of the keto–enol tautomerization in the ground state in which the transient tautomers are formed by thermal fluctuations. In addition, excited electronic states of the transient tautomers were computed in order to gain insight into the excited state properties. Due to computational feasibility, the *tert*-butyl group was excluded and 4-methoxydibenzoylmethane, which represents a reduced model of avobenzone, was studied. The electron-donating nature of the *tert*-butyl group decreases the energies of the $\pi\pi^*$ state and therefore, the calculated $\pi\pi^*$ energies will be blue-shifted compared to those of AB. Nevertheless, the lack of the *tert*-butyl group does not significantly alter the thermal equilibrium between the tautomers since it is largely determined by the dibenzoylmethane moiety.

In this work, two mechanisms for the keto–enol tautomerization depicted in Fig. 1 are postulated. In the first mechanism, the hydroxyl group of the chelated enol tautomer rotates, which results in hydrogen bond breakage and the formation of the non-chelating enol **2** tautomer. The second step in this process is a rotation about the single C₁–C₂ bond, which leads to the formation of a conformer labeled as rotamer **s**. Furthermore, the hydrogen of the O₂–H hydroxyl group of rotamer **s** rotates, which results in the creation of rotamer **s2**. In the last step, this hydrogen atom shifts to the C₁ atom resulting in the formation of the keto **s** tautomer. The second mechanism begins with the rotation of the hydroxyl

group, which is identical to the first step of the first mechanism. On the other hand, this rotation in the second mechanism is followed by another rotation about the C₁=C₃ double bond.

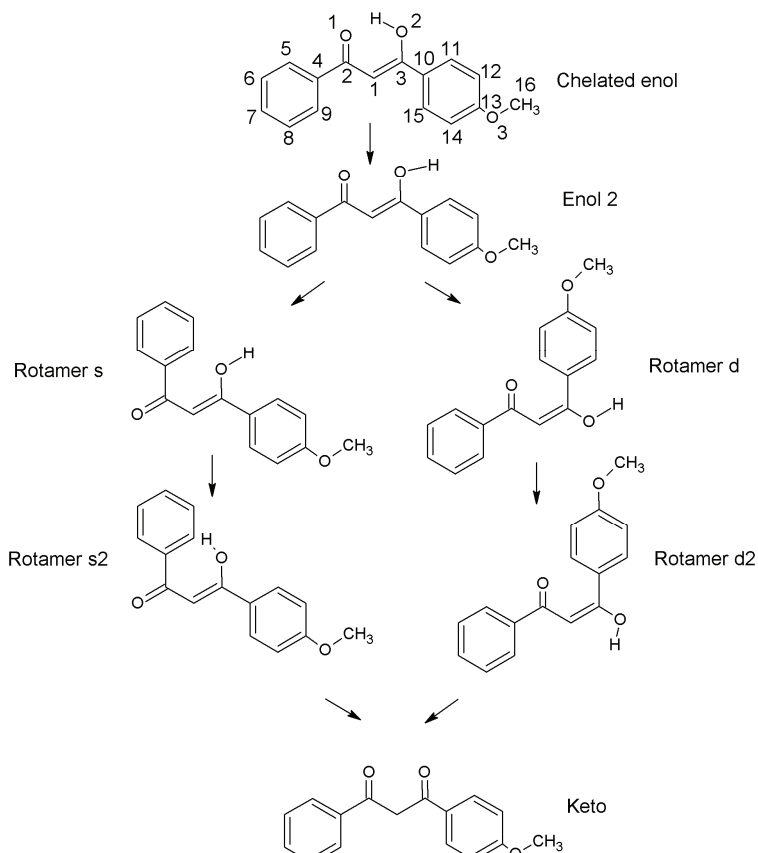


Fig. 1. Schematic representation of the two possible mechanisms of keto–enol tautomerization: rotation about the single C₁–C₂ bond (left pathway) and rotation about the double C₁=C₃ bond (right pathway). Atom labeling used in this work is presented in the chelated enol structure.

The last two steps of the second mechanism are similar to the ones in the first mechanism. Thus, they involve the creation of rotamer **d2** and finally keto **d** tautomer. Since there are two oxygen atoms O₁ and O₂, there are two sets of enol conformers depending whether the hydrogen atom is bound to O₁ or O₂ atom. The performed computation revealed that the free energy difference between the two chelated enol conformers is only 0.7 kJ mol⁻¹, which is much smaller than the accuracy of the used method. Thus, these conformers were regarded as equivalent and only the enol tautomers in which the hydrogen atom is bound to

the O₂ atom were considered. Similarly, the free energy difference between two enol conformers in which the methoxy group was rotated was found to be 1.2 kJ mol⁻¹ and thus, the tautomers with a rotated methoxy group were not examined.

COMPUTATIONAL DETAILS

In the present work, all calculations were performed with the Gaussian 09 program package.²³ Geometry optimizations and vertical excitation energies were calculated using density functional theory with CAM-B3-LYP functional with TZVP basis set. Ultrafine grid was used for numerical integrations. Gibbs energies were calculated by adding electronic energy to thermal contributions from translational, rotational and vibrational motion and assuming standard conditions for temperature and pressure. The rotational and vibrational motion was approximated by the harmonic rigid-rotor approximation. All computations were performed for vacuum.

RESULTS AND DISCUSSION

The ground state geometries

The optimized ground state structures and bond lengths of all tautomers in the keto–enol tautomerization mechanisms are presented in Figs. 2 and 3. The chelated enol geometry was found to be slightly non-planar. The hydrogen atom attached to the O₂ atom points toward the oxygen atom of the O₁=C₂ group establishing an intramolecular hydrogen bond the length of which is 1.55 Å. The C₂=O₁ bond is a typical double bond whereas the C₃=O₂ bond has a single bond character. Their lengths are 1.25 and 1.33 Å, respectively. The C₁–C₂ bond is longer than the C₁–C₃ bond by 0.06 Å. The average C–C bond length in benzene rings is 1.39 Å. The calculated bond lengths of the chelated enol tautomer are in good agreement with the values obtained with the M06-2X functional.²¹

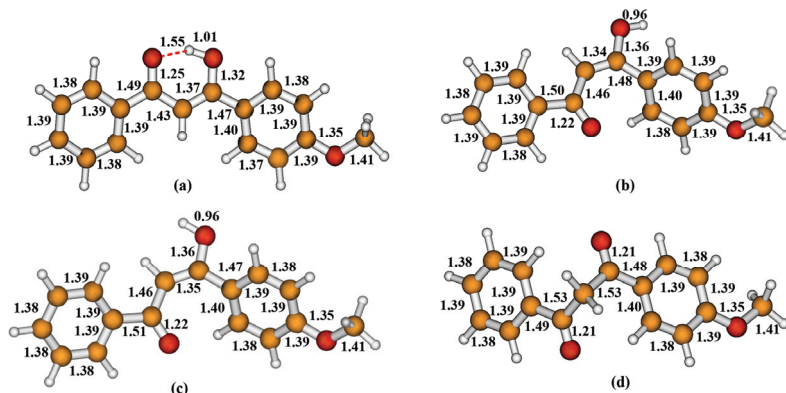


Fig. 2. The optimized structures of the chelated enol (a), rotamer **d** (b), rotamer **d2** (c) and keto **d** (d) tautomers in the ground state.

Now the optimized geometry of the enol 2 tautomer (*cf.* Fig. 3a) is discussed. Due to the rotation of the hydroxyl group, the intramolecular hydrogen

bond breaks, this results in an increment of the C₂–C₁–C₃ angle by 5.5° relative to chelated enol form. The benzene ring with an attached OCH₃ group was found to be displaced out of plane. In addition, the dihedral angle C₁–C₃–C₁₀–C₁₅ amounts to 40.8°. This value is significantly larger than that computed for the chelated enol tautomer (14.9°). Comparison of bond lengths found for the chelated enol with those found for the enol **2** structures revealed that the largest difference was found for the C₁–C₂ bond, which elongates by 0.15 Å in the enol **2** structure. In addition, C₂=O₁ and C₃=O₂ bonds gain more double and single bond character, respectively. Thus, it is predicted that the O₁–C₂–C₁–C₃–O₂ ring loses its stability in the enol **2** structure due to the absence of the electron delocalization that was present in the chelated enol.

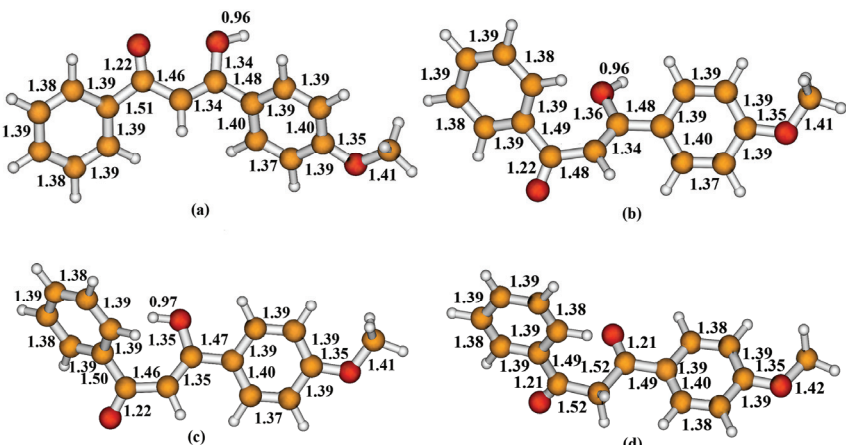


Fig. 3. The optimized structures of the enol **2** (a), rotamer **s** (b), rotamer **s2** (c) and keto **s** (d) tautomers in the ground state.

The optimized ground-state structures of rotamer **d** and rotamer **s** are characterized by significant deviations from the planar structure since they were formed by rotation about single C₂–C₁ (rotamer **s**) and double C₁=C₃ (rotamer **d**) bonds. Furthermore, these rotations lead to a significant change of the C₄–C₂–C₁–C₃ dihedral angle. In the rotamer **d**, its value is 163.2° while in rotamer **s**, it amounts to –40.1°. The largest bond length change occurs for the C₁–C₂ bond, which elongates by 0.02 Å in the rotamer **S** tautomer. Similarly, the optimized geometries of rotamers **d2** and **s2** were found to be distorted and non-planar. Comparison of the bond lengths for these optimized geometries shows that there are no significant differences between these two species. On the other hand, the C₄–C₂–C₁–C₃ dihedral angles are 163.1 and –29.4° in rotamers **d2** and **s2**, respectively.

Interestingly, two different keto structures were found, which are labeled keto **s** and keto **d**. The oxygen atoms in these structures are in *trans* arrangements. The *cis* arrangement is not stable due to repulsion of oxygen nonbonding electrons and they transform to the *trans* arrangements. The dibenzoylmethane moiety of the optimized geometry of the keto **d** tautomer is symmetric while in the case of keto **s**, it is characterized by a twisted geometry. There are no significant bond length differences between these two keto structures. The maximal difference was found to be 0.01 Å. In addition, the largest difference between these two tautomers was found for the C₄–C₂–C₁–C₃ dihedral angle. The value of this angle is 77.7 and –78.9° for keto **d** and **s**, respectively.

Electronic and Gibbs energies

The differences in zero-point corrected electronic energies and standard Gibbs energies of all tautomers with respect to the chelated enol tautomer in the ground state are given in Fig. 4. The thermal and entropic corrections increase the electronic energy of the chelated enol tautomer by 120.2 kJ mol⁻¹. Both keto–enol tautomerization mechanisms begin with the breaking of the hydrogen bond

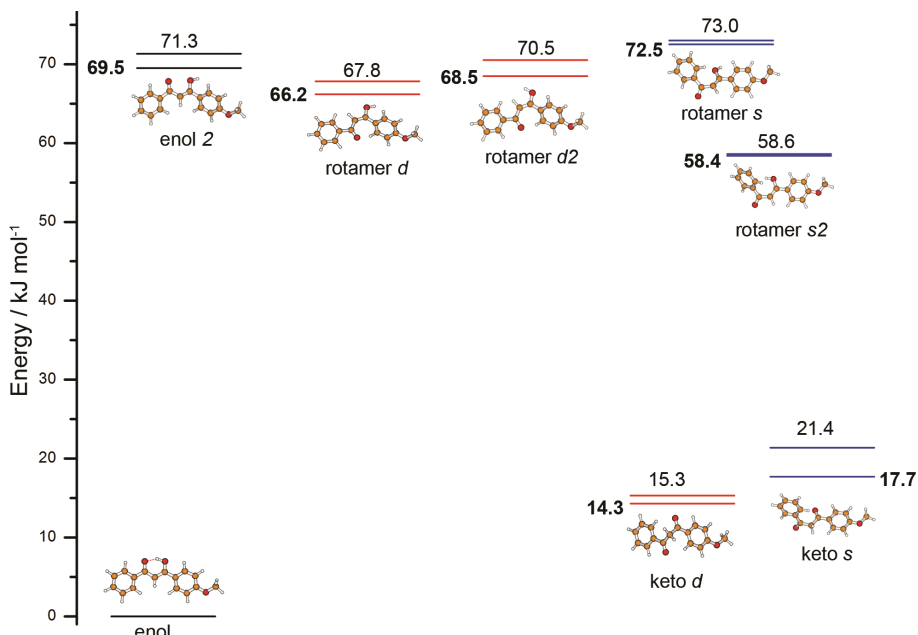


Fig. 4. Zero-point corrected differences in the electronic energy and Gibbs energy (bold numbers) between tautomers with respect to the chelated enol in the ground state (in kJ mol⁻¹). The difference between the Gibbs energy and electronic energy of the enol form is 120.2 kJ mol⁻¹. Structures involved in the keto–enol tautomerization mechanism that involve rotation about the single and double bond are colored blue and red, respectively.

and formation of the enol **2** tautomer. The calculated electronic and Gibbs energy differences between chelated enol and the enol **2** tautomers amount to 71.3 and 69.5 kJ mol⁻¹, respectively. This large energy change stems from the breaking of the intramolecular hydrogen bond and a loss of related electron delocalization in the O₁—C₂—C₁—C₃—O₂ ring of the chelated enol form. Thus, the hydrogen bond breakage is a highly endothermic process and for this reason, the chelated enol structure is always observed in thermal equilibrium. The next intermediate tautomer is formed by a rotation about the single C₁—C₂ and double C₂=C₃ bond resulting in rotamers **s** and **d**, respectively. Since rotamer **s** is formed by rotation about a single bond, it is expected that its rotation barrier would be much smaller than in the case of rotamer **d**. Comparison of the electronic and Gibbs free energies of rotamers **d** and **s** reveals that rotamer **d** is located energetically below rotamer **s** by approximately 5 kJ mol⁻¹. In addition, the rotamer **d** tautomer is approximately 3 kJ mol⁻¹ more stable than the enol **2** tautomer. On the other hand, rotamer **s** is 2 kJ mol⁻¹ less stable than the enol **2** tautomer. The thermodynamic equilibrium constant for the conversion of rotamer **d** to **s** is 0.12. Thus, once rotamer **d** is formed, it is thermodynamically possible to obtain rotamer **s**. Interestingly, it was found that a rotation of the hydroxyl group stabilized rotamer **s** by approximately 24 kJ mol⁻¹ but destabilized rotamer **d** by 2 kJ mol⁻¹. Thus, rotamer **d2** is less stable than rotamer **s2**.

The formation of the keto form in the last step is a strongly exothermic process in both mechanisms. In the case of the mechanism that involves the rotation about the single bond, the formation of the keto tautomer is followed by the release of 37 kJ mol⁻¹. Even more energy (55 kJ mol⁻¹) is released in the mechanism that involves the rotation about the double bond. The Gibbs energies of the keto **s** and **d** tautomers are approximately 15 and 21 kJ mol⁻¹ larger than those of the chelated enol, respectively. Based on these numbers, the equilibrium constant for the transformation of the chelated enol to the keto tautomer was computed to be only 0.002.

The largest difference in two tautomerization mechanisms concerns the energy barriers. The rotation around the single bond is energetically significantly less expensive than the rotation around the double bond. Thus, the thermal tautomerization is expected to occur *via* single bond rotation.

Vertical electronic excitation spectra

Now, the singlet and triplet vertical electronic excitation spectra calculated from the optimized ground state structures are discussed. The considerations were restricted to the structures that are important in the tautomerization mechanism based on the rotation around the double bond since the excitation of an electron from the π to the π^* orbital localized on the C₁=C₃ double bond would weaken this bond. The singlet and triplet excited state energies and oscillator

strengths for the chelated enol, the keto **d** and rotamer **d** tautomers computed at the optimized ground state geometries are shown in Fig. 5. The selected frontier Kohn–Sham orbitals of the chelated enol, keto and rotamer **d** are presented in Figs. 6–8, respectively. The first excited singlet state of the chelated enol tautomer has $\pi\pi^*$ character and comes from HOMO to LUMO excitation. Its excitation energy is 4.09 eV and it is strongly dipole allowed with an oscillator strength of 0.91. The calculated energy is approximately 0.6 eV higher than the experimentally observed energy in acetonitrile.¹⁷ This discrepancy comes largely from neglecting the solvent effects and the *tert*-butyl group, although there is also a contribution from the calculation method of the electronic structure. On the other hand, the second and third singlet excited states have negligible oscillator strengths. The energies of the second and third excited singlet states are 4.17 and 4.98 eV, respectively.

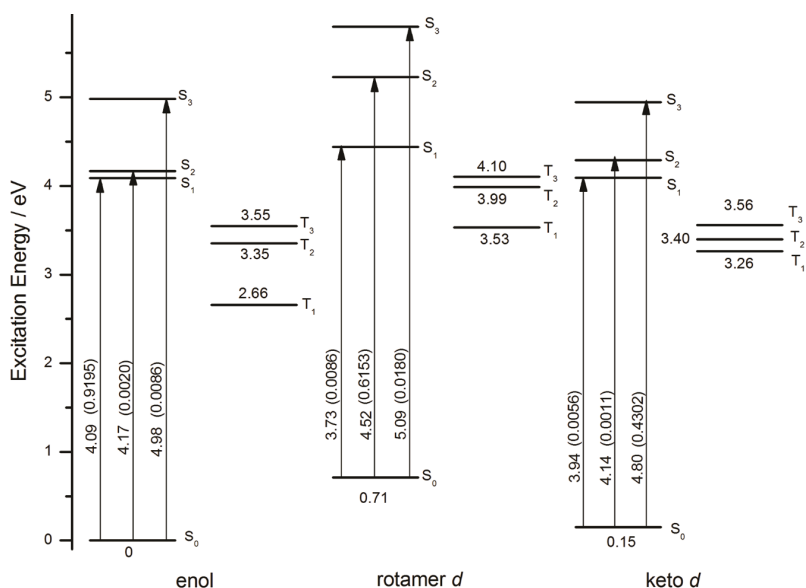


Fig. 5. Vertical electronic excitation spectrum of three tautomers of AB at the ground state geometry with respect to the chelated enol form. All energies are in eV. The calculated oscillator strengths are displayed in brackets.

The second excited singlet state has $\pi\pi^*$ character and comes from HOMO–4→LUMO and HOMO–5→LUMO transitions. On the other hand, the third excited singlet state is largely formed from the HOMO–3→LUMO+2 transition. The lowest triplet state dominantly results from HOMO–1→LUMO excitation and exhibits $\pi\pi^*$ character. Its excitation energy is 2.66 eV, which is 1.43 eV lower than the energy of the S_1 state. The second and third triplet states also have $\pi\pi^*$ character. Their energies are 3.35 and 3.55 eV. Therefore, three triplet states

are located below the S_1 state in the enol tautomer. Since all these triplet states have the same orbital character as the S_1 state, it is not expected that intersystem crossing from the S_1 to the triplet states would be fast.

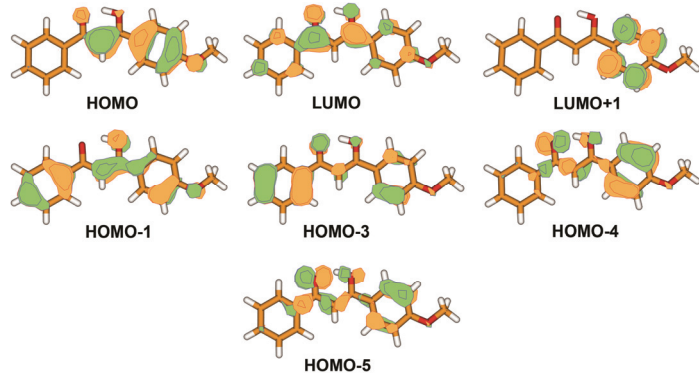


Fig. 6. Selected frontier Kohn–Sham orbitals of the chelated enol tautomer.

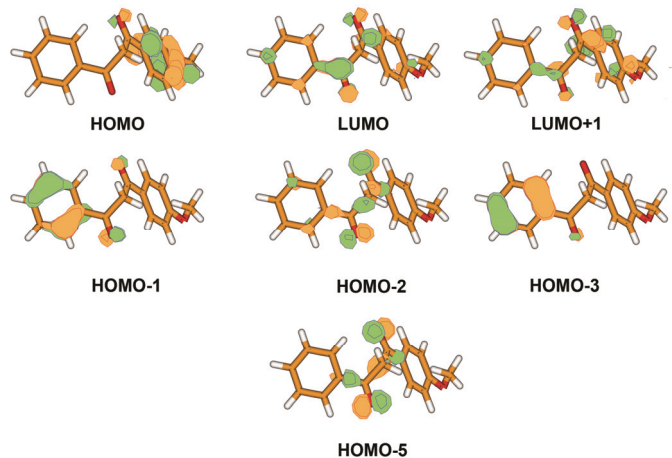


Fig. 7. Selected frontier Kohn–Sham orbitals of the keto tautomer **d**.

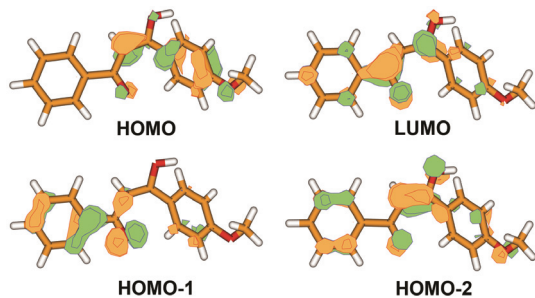


Fig. 8. Selected frontier Kohn–Sham orbitals of the rotamer **d**.

In order to discuss the excited states of the keto **d** tautomer, it should be remembered that the ground state of the keto **d** tautomer is 0.15 eV higher than that of the enol tautomer. Since the geometry of the keto **d** tautomer is non-planar, there is mixing of nonbonding and π orbitals. The two lowest excited singlet states of the keto **d** tautomer are dark $n\pi^*$ states. Their excitation energies are 3.94 and 4.14 eV. The first excited singlet state comes from the HOMO-2 \rightarrow LUMO transition, while the second state comes from the HOMO-5 \rightarrow LUMO transition. The energy of the third excited singlet state is 4.80 eV and the oscillator strength value of 0.43 indicates that this state is strongly dipole allowed. Its computed energy is in good agreement with the experimental value of 4.68 eV.¹⁷ The S_3 state consists of HOMO \rightarrow LUMO and HOMO \rightarrow LUMO+1 excitations. Taking into account the ground state energy, it is approximately 0.85 eV higher than the bright state of the chelated enol tautomer. As for the chelated enol tautomer, the first three triplet states of the keto **d** tautomer are below the first excited singlet state. The T_1 state of keto **d** is of $\pi\pi^*$ character and results mostly from HOMO \rightarrow LUMO and HOMO \rightarrow LUMO+1 excitations. Vertical excitation energy to the T_1 state is 3.11 eV. The energies of the second and third states are 3.25 and 3.41, respectively. They are of mixed $n\pi^*$ and $\pi\pi^*$ character. The T_2 state comes mainly from HOMO-1 \rightarrow LUMO and HOMO-3 \rightarrow LUMO excitations. On the other hand, the T_3 state results from HOMO-2 \rightarrow LUMO excitation. Comparison of the vertical excitation energies of the triplet states of the chelated enol and keto **d** tautomers reveals that the T_1 state of the keto **d** tautomer is above the T_1 state of the chelated enol but the T_2 and T_3 states are approximately of the same energy.

In the case of rotamer **d**, the bright state is the second excited state. Its excitation energy is 4.52 eV and it dominantly consists of HOMO \rightarrow LUMO excitations, but there is also a small contribution from HOMO-1 \rightarrow LUMO and HOMO-2 \rightarrow LUMO transitions. The energies of the S_1 and S_3 states are 3.73 and 5.09 eV, respectively. The T_1 state of the rotamer **d** has $\pi\pi^*$ character and dominantly results from HOMO \rightarrow LUMO and HOMO-2 \rightarrow LUMO excitations. The energy required for this transition is 2.82 eV. The T_2 and T_3 states have mixed $n\pi^*$ and $\pi\pi^*$ character. Their energies are 3.28 and 3.39 eV, respectively. Interestingly, the energies of the first three triplet states of rotamer **d** are higher than the corresponding energies of the chelated enol and the keto **d** tautomers.

The geometries of the first excited singlet state

The nuclear arrangements of the first excited singlet electronic state of the chelated enol, keto **d** and rotamer **d** tautomers were optimized. Their geometries with bond lengths are presented in Fig. 9. The chelated enol tautomer has almost planar geometry in the S_1 state. The hydrogen bond length in the S_1 state is 0.07 Å shorter than in the ground state. Comparing the bond lengths in the S_1 and the ground state, it was found that the most significant change occurs for the C₁-C₂

bond (+0.13 Å). The optimized S_1 state has $\pi\pi^*$ character that results from HOMO \rightarrow LUMO and HOMO-1 \rightarrow LUMO excitations. Its adiabatic electronic energy is 3.93 eV. Thus, the S_1 state relaxes by 0.16 eV upon photoexcitation from the ground state. The oscillator strength for the transition to the ground state is 0.8866. Fluorescence of the enol form was observed in solid ethanol but not in room temperature solutions. The origin of the fluorescence was estimated to be 3.17 eV,¹³ which is 0.76 eV lower than the computed energy. This large difference could be attributed to the same reasons as in the case of the vertical excitation energy.

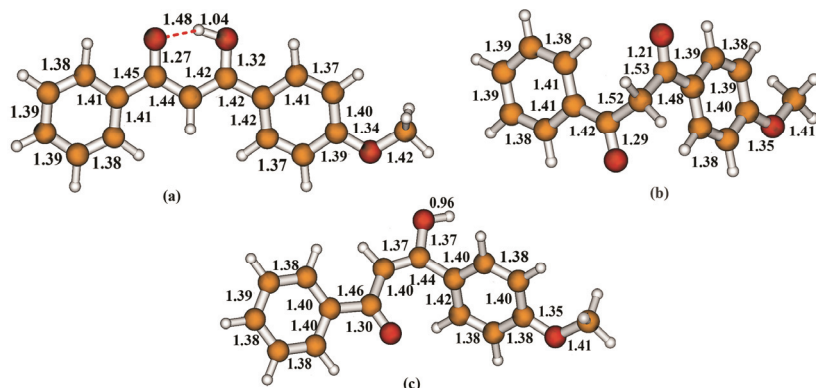


Fig. 9. The optimized structures of the chelated enol (a), keto **d** (b) and rotamer **d** (c) tautomers in the S_1 state.

The lowest excited singlet state of the keto **d** tautomer has $n\pi^*$ character. The maximum bond length elongation with respect to the ground state was found for the C₂-O₁ bond and it amounts to 0.08 Å. Besides the bond length changes, an additional difference between the keto **d** ground and S_1 states was found for the C₄-C₂-C₁-C₃ dihedral angle. This angle differs by 7°. The electronic adiabatic energy of the S_1 state is 3.87 eV. Taking into account the ground state energy, it is slightly above the S_1 energy of the chelated enol tautomer.

The lowest excited singlet state of the rotamer **d** tautomer has $n\pi^*$ character. The most prominent characteristic of the geometry of its S_1 state is that the C₂-O₁ bond is elongated by 0.08 Å compared to the ground state geometry. In addition, the C₄-C₂-C₁-C₃ dihedral angle in the S_1 state is larger by 14.5° with respect to the ground state value. The electronic adiabatic energy of the S_1 state is 3.17 eV.

The geometries of the first excited triplet state

The optimized structures of the enol, keto **d** and rotamer **d** tautomers in the first excited triplet electronic state are displayed in Fig. 10. The T₁ geometry of the enol tautomer is characterized by a planar structure, similar to its geometries

in the ground and S₁ state. The most significant bond length change in the T₁ state relative to the ground state is the elongation of the hydrogen bond by 0.14 Å. Moreover, comparing to its length in the S₁ state, it is elongated by 0.21 Å. The T₁ state is of $\pi\pi^*$ character and results from HOMO→LUMO excitation. Its electronic adiabatic energy is 1.93 eV. This energy is 2.00 eV lower than the adiabatic energy of the S₁ state.

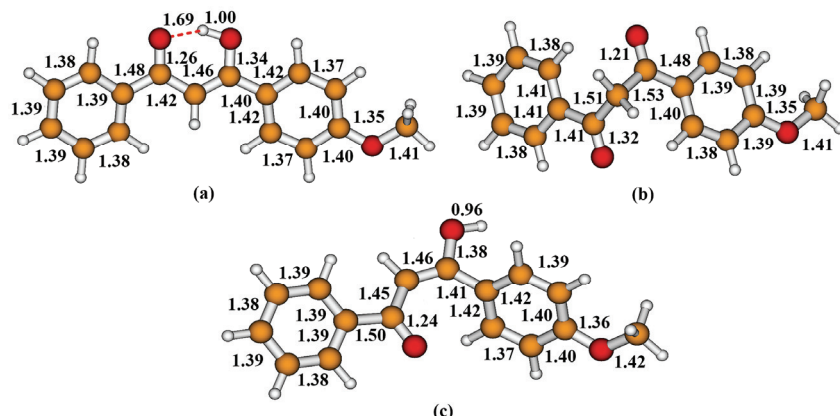


Fig. 10. The optimized structures of the chelated enol (a), keto **d** (b) and rotamer **d** (c) tautomers in the T₁ state.

The optimized geometry of the keto **d** tautomer in the T₁ state has $n\pi^*$ character. The maximum bond length change with respect to the ground state occurs for the C₂=O₁ bond. This bond is elongated in the T₁ state by 0.11 Å. In addition, it is 0.08 Å longer than in the S₁ state. The C₄–C₂–C₁–C₃ dihedral angle of the keto **d** tautomer is smaller by 5.5° compared to the ground state value. Vertical excitation energy to the T₁ state was found to be 2.56 eV, which is 1.13 eV lower compared to that for the S₁ state geometry. The minimum of the T₁ state of the keto **d** tautomer is 0.64 eV above that of the chelated enol.

The lowest triplet state geometry of rotamer **d** was found to be non-planar. It originates from a HOMO→LUMO transition and has $\pi\pi^*$ character. Compared to the ground state geometry, the maximum bond length difference was found for the C₁–C₃ bond. It is elongated by 0.12 Å in the triplet state. In addition, the C₄–C₂–C₁–C₃ dihedral angle is increased by 12.2°. Compared to the S₁ state, the most significant bond length change occurs also for the C₁–C₃ bond.

CONCLUSIONS

Avobenzone is the most widely used UV-A filter in cosmetic sunscreens. Its keto–enol tautomerization is complex due to appearance of several transient tautomers. In this contribution, two thermal pathways of a reduced model of avobenzone were examined. The first includes rotation about a single C–C bond,

whereas the second proceeds *via* a rotation about a double C=C bond. The studied tautomers were the chelated and non-chelated enol, rotamers **s**, **s2**, **d**, **d2**, and the keto **s** and **d** tautomers. Breaking of the intramolecular hydrogen bond in the chelated enol is a highly endothermic process that is followed by loss of electron delocalization in avobenzone. The most stable transient tautomer was found to be rotamer **s2**. The equilibrium constant for transformation of the chelated enol to the keto tautomer was calculated to be 0.002. The obtained results show that the bright state in the chelated enol is the first excited singlet state, the second in rotamer **d** and the third state in the keto form. In the latter two tautomers, the S₁ states have nπ* character. The lowest excited triplet states of chelated enol and rotamer **d** have ππ* character whereas in the case of the keto tautomer, it has nπ* character.

Acknowledgements. The authors acknowledge the Ministry of Education, Science and Technological Development of the Republic of Serbia for the financial support (Contract No. 172040). The numerical simulations were run on the PARADOX cluster at the Scientific Computing Laboratory of the Institute of Physics, Belgrade, supported in part by the Ministry of Education, Science, and Technological Development of the Republic of Serbia under Project No. ON171017.

ИЗВОД

ОТКРИВАЊЕ МЕХАНИЗМА ТЕРМАЛНЕ ТАУТОМЕРИЗАЦИЈЕ АВОБЕНЗОНА ПОМОЋУ КВАНТНОХЕМИЈСКИХ ПРОРАЧУНА

МАРКО КОЛИЋ, МИЛЕНА ПЕТКОВИЋ И МИХАЈЛО ЕТИНСКИ

Факултет за физичку хемију, Универзитет у Београду, Студентски трг 12–16,
б. тр. 47, 11158 Београд

Авобензон (1-(4-*tert*-бутилфенил)-3-(4-метоксифенил)пропан-1,3-дион) је један од најкоришћенијих UV-A филтера у козметичким средствима за сунчање. Реактивност авобензона је комплексна и изазовна за разумевање због присуства прелазних таутомера. Испитивани су енолни, ротамерни и кето таутомери редукованог модела авобензона који су укључени у кето-енолну таутомеризацију. Постулирана су два термална таутомеризациони механизма и продискутоване су њихове интермедијерне структуре. Израчунате вертикалне и адијабатске ексцитационе електронске енергије обезбеђују додатни увид у особине побуђених стања таутомера.

(Примљено 31. маја, ревидирано 17. јула, прихваћено 21. септембра 2016)

REFERENCES

1. M. M. Petković, M. R. Etinski, M. M. Ristić, *Hem. Ind.* **67** (2013) 203
2. M. M. Ristić, M. Petković, M. Etinski, *J. Serb. Chem. Soc.* **77** (2012) 1037
3. G. P. Pfeifer, A. Besaratinia, *Photochem. Photobiol. Sci.* **11** (2012) 90
4. N. A. Shaath, *Photochem. Photobiol. Sci.* **9** (2010) 464
5. D. Veierov, T. Bercovici, E. Fischer, Y. Mazur, A. Yogevev, *J. Am. Chem. Soc.* **99** (1977) 2723
6. H. Gonzenbach, T. J. Hill, T. G. Truscott, *J. Photochem. Photobiol., B* **16** (1992) 377
7. S. Tobita, J. Ohba, K. Nakagawa, H. Shizuka, *J. Photochem. Photobiol., A* **92** (1995) 92 61
8. W. Schwack, T. Rudolph, *J. Photochem. Photobiol., B* **28** (1995) 28 229

9. I. Andrae, A. Bringhen, F. Böhm, H. Gonzenbach, T. Hill, L. Mulroy, T. G. Truscott, *J. Photochem. Photobiol., B* **37** (1997) 147
10. A. Cantrell, D. J. McGarvey, *J. Photochem. Photobiol., B* **64** (2001) 117
11. A. Aspée, C. Aliaga, J. C. Scaiano, *Photochem. Photobiol.* **83** (2007) 481
12. G. Mturi, B. S. Martincigh, *J. Photochem. Photobiol., A* **200** (2008) 410
13. A. Kukuchi, N. Oguchi, M. Yagi, *J. Phys. Chem., A* **113** (2009) 13492
14. C. Paris, V. Lhiaubet-Vallet, O. Jiménez, C. Trullas, M. A. Miranda, *Photochem. Photobiol.* **85** (2009) 178
15. M. Yamaji, M. Kida, *J. Phys. Chem., A* **117** (2013) 1946
16. L. P. da Silva, P. Ferreira, D. Duarte, M. Miranda, J. E. da Silva, *J. Phys. Chem., A* **118** (2014) 1511
17. A. Kukuchi, N. Oguchi-Fujiyama, K. Miyazawa, M. Yagi, *Photochem. Photobiol.* **90** (2014) 511
18. P. K. Verma, F. Koch, A. Steinbacher, P. Nuernberger, T. Brixner, *J. Am. Chem. Soc.* **136** (2014) 14981
19. A. D. Dunkelberger, R. D. Kieda, B. M. Marsh, F. F. Crim, *J. Phys. Chem., A* **119** (2015) 6155
20. P. K. Verma, A. Steinbacher, F. Koch, P. Nuernberger, T. Brixner, *Phys. Chem. Chem. Phys.* **17** (2015) 8459
21. M. Petković, M. Etinski, *RSC Adv.* **4** (2014) 38517
22. J. Zawadiak, M. Mrzyczek, *Spectrochim. Acta, A* **75** (2010) 925
23. Gaussian 09, revision D.01, Gaussian, Inc., Wallingford, CT, 2013.